Journal of Biomedical Optics

SPIEDigitalLibrary.org/jbo

Advantages of full spectrum flow cytometry

Claire K. Sanders
Judith R. Mourant

SPIE

Advantages of full spectrum flow cytometry

Claire K. Sanders and Judith R. Mourant
Los Alamos National Laboratory, Bioscience Division, P.O. Box 1663, MS M888, Los Alamos, New Mexico 87544

Abstract. A charge coupled device-based flow-cytometer for the measurement of full spectra was implemented and characterized. The spectral resolution was better than 1.5 nm and the coefficient of variation for fluorescence from flow check beads was 5% or better. Both cell and bead data were analyzed by fitting to measured component spectra. Separation of flow check and align flow beads, which have similar spectra, was nearly identical whether using a spectral analysis or a scatter analysis. After mixing, cells stained with ethidium bromide or propidium iodide were measured at different timepoints. The contribution of these 12 nm separated emission spectra could be separately quantified and the kinetic process of the samples becoming homogeneous due to fluorophor dissociation and rebinding was observed. Principle component analysis was used to reduce noise and alternating least squares (ALS) was used to analyze one set of noise-reduced cell data without knowledge of the component spectra. The component spectra obtained via ALS are very similar to the measured component spectra. The contributions of ethidium bromide and propidium iodide to the individual spectra are also similar to those obtained via the spectral fitting procedure. [DOI: 10.1117/1.JBO.18.3.037004]

Keywords: cancer detection; immunology; flow cytometry; multivariate curve resolution; compensation; alternating least squares.

Paper 130007R received Jan. 5, 2013; revised manuscript received Feb. 14, 2013; accepted for publication Feb. 15, 2013; published online Mar. 11, 2013.

1 Introduction

Measurement of fluorescence in conventional flow cytometry is performed with bandpass and/or long-pass filters and photomultiplier tubes (PMTs) to measure fluorescence emission. When only a small number of fluorescence signals are being measured, and any background fluorescence is well-characterized, the use of bandpass filters provides an effective, and relatively simple-to-implement, measurement system. However, when multiple fluorophors are present, the background varies, or emission spectra vary due to sample conditions, conventional measurements with bandpass filters can be difficult to interpret and can potentially lead to erroneous results. Furthermore, to account for the overlap of emission spectra in the detection channels, an additional number of samples equal to the number of fluorescence parameters measured must be prepared and run.

We have implemented a full-spectrum flow cytometry system that measures forward-scatter, side-scatter and a fluorescence spectrum for each particle or cell. This paper demonstrates the ability of our system to distinguish and quantify fluorescence from highly overlapping fluorophors even when those fluorophors are staining the same cell.

Full-spectral measurement enables data analysis methods not previously used in flow cytometry. This paper also demonstrates that full-spectral measurement has the potential to greatly reduce or eliminate the number of samples needed to be measured to account for fluorescence overlap.

An instrument capable of measuring full spectra and accompanying new analysis methods would enable rapid, higher-order multiparametric analyses. Such analyses could enable new studies in complex systems, such as the immune system, where fluorescently labeled antigens are used to identify T-cell lineages, as well as B-cell and natural killer subsets.[1] Additionally, full-spectral measurements could simplify applications, such as flow cytometric fluorescence resonance energy transfer (FRET) or flow cytometric internal pH measurements.

Address all correspondence to: Claire K. Sanders, Los Alamos National Laboratory, P.O. Box 1663 MS M888, Bioscience Division, Los Alamos, New Mexico 87544. Tel: (505) 665-1190; E-mail: csanders@lanl.gov

2 Methods

The goals of our experiments were to demonstrate that the spectral instrument is capable of differentiating particles with similar, but not identical spectra, and quantifying the relative concentrations of spectrally similar dyes in a given particle or cell. The first experiment uses polystyrene microspheres with highly overlapping spectra. The spheres are separated based on their spectra only. We then compare the accuracy of this separation based on spectra with a separation based on scatter signals. The second experiment uses cells stained with two dyes with very similar spectra. Measurements are made of singly stained cells and then the cells are mixed together. Over time, the dyes dissociate from their substrate (DNA) and each cell is stained by both dyes. By measuring at a few time points, this kinetic process can be observed.

2.1 *Optical Measurement System*

A schematic of the instrument is shown in Fig. 1. A 488-nm laser (Innova 200, Coherent Inc., Santa Clara, California) is focused by two cylindrical lenses onto a BD FACSCalibur flow cell with attached light collection lens (Becton Dickinson, San Jose, California). Side-scattered light is transmitted through a dichroic beam splitter (FF505-SD, Semrock, Rochester, New York) onto a Hamamastu (Bridgewater, New Jersey) R636-10 PMT. Fluorescence is reflected by the same dichroic, passed through a dove prism, dispersed by a spectrometer (f1.8i Holospec using a HVG-590 grating, Kaiser Optical Systems Inc., Ann Arbor, Michigan), and detected with a 1600×200 pixel electron multiplying charge coupled device (EMCCD) (Newton model DU970N-UVB, Andor Technology PLC., South Windsor, Connecticut). Forward-scattered light is quantified with an amplified detector (PDA100A,

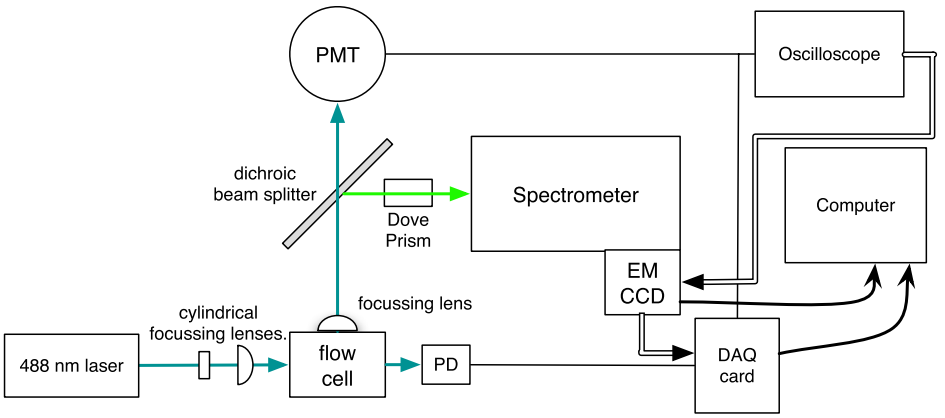

Fig. 1 A schematic of the spectral flow cytometer. Light is represented by colored lines, analog signals by narrow black lines, TTL pulses by two narrowly separated black lines and USB cables by double thick black lines. Components are described in the text.

Thor Labs, Newton, New Jersey) equipped with a beam stop to block direct laser light.

The output of the PMT (i.e., the side-scatter signal) is split and one part sent to a simple noninverting amplifier (OPA37GP) with its output going to a USB data acquisition (DAQ) card (9221, National Instruments, Austin Texas). The other part is sent to a Tektronix (Beaverton, OR) 2445B oscilloscope for real-time visualization of side scatter and generation of a transistor-transistor logic (TTL) trigger for the EMCCD camera from the side scatter signal. Since the PMT generates a current of electrons, the side-scatter voltage measured by the high impedance oscilloscope and amplifier is negative. The camera is controlled with Newton Andor Software and the spectra from the camera are sent directly to the computer via a USB connection. The camera sends out a TTL signal when it is collecting data and this goes directly to the DAQ card without amplification. The output of the forward-scatter detector is amplified with the same type of amplifier as the side-scatter signal and sent to the DAQ card. Collection of data from the DAQ card via a USB connection is performed with Igor Pro software (Wavemetrics, Tigard, Oregon) including NiDAQmx Tools.

A "home-built" pressure system is used to provide sheath flow and a Harvard Apparatus (Holliston, Massachusetts) PHD 2000 syringe pump is used to generate sample flow. Flowing particles are hydrodynamically focused in the BD FACSCalibur flow cell.

The spectral resolution was measured by placing a 532-nm laser in the beam path and examining the width of the scattered laser line. Spectral calibration was performed using spectral calibration lamps and a 532-nm laser.

2.2 *Samples*

Fluorescent polystyrene microspheres were used as controls for instrument setup, as well as for demonstration of the instrument's ability to use spectral properties to separate particles with similar spectra. Two types of microspheres were chosen for their different sizes and spectral characteristics: flow check fluorospheres (Beckman-Coulter) are 10 μm in diameter and have a bright, two-peak emission spectra. Align flow beads (Invitrogen) are 2.5 μm in diameter and have a simpler emission peak. Microspheres were analyzed individually so that pure populations could be characterized, the samples were then mixed and the populations separated in software.

Tumorigenic rat fibroblast, MR1, cells were grown in Dulbecco's Modified Eagles Medium (DMEM) supplemented with 5% (v/v) of fetal calf serum (HyClone Thermo Fisher Scientific, Waltham, Massachusetts), 100 units/ml of penicillin, and 100 μg/mL of streptomycin. To obtain cell suspensions for staining and subsequent flow-cytometric analysis, cells were harvested from monolayer cultures in the exponential phase of growth by treatment with 0.25% trypsin in a phosphate-buffer (pH 7.4) containing 1 mM EDTA and 25 mM HEPES. Cells were then fixed in 70% EtOH/30% phosphate buffered saline (PBS) and stored at −20°C until use.

MR1 cells were stained at a concentration of 2 to 3×10^6 cells/ml with 5 μg/mL (7.5 μM) propidium iodide (PrI) and/or 3 μg/mL (7.6 μM) ethidium bromide (EB) in PBS containing 50 μg/mL RNase A. These fluorophors were chosen to be a stringent test of the spectral deconvolution abilities of our measurement and analysis techniques. These concentrations were chosen so that the concentration of molecules would be similar for the two stains. Cells were incubated in staining solution for 30 min at 37°C and stored for a short period at 4°C if not used immediately. Single-stained samples were split in half; with one half being used for measurement while the other half was used for mixing samples stained with EB and PrI. Single-stained cell samples were washed before data collection, or before mixing, in order to reduce free dye in the solution. [Significant fluorescence from free dye was measured when unwashed samples were analyzed and these spectra are shown in Fig. 2(b).] Cell suspensions were centrifuged at 3000 rpm for 1 min in a microcentrifuge, the supernatant was removed and PBS was added. After a 5-min wait the wash step was repeated.

2.3 *Data Collection*

The sheath was 1× PBS with no calcium/magnesium [Hyclone Dulbeccos PBS (Powder)] and was run at 5-6psi. The samples were loaded into syringes and injected into the system at a rate of 5 to 15 μl/ min. Laser intensity at the sample was 7 mW at 488 nm. The camera was binned to four bins vertically and 400 bins horizontally, the majority of fluorescence was seen in one vertical bin, and the spectral information was collected along the horizontal axis. The camera was set to a readout rate of 2.5 MHz and the sample integration time was 60 μs. Flow check fluorospheres were collected every day that cells were run to monitor instrument performance. For microspheres and cells, spectral

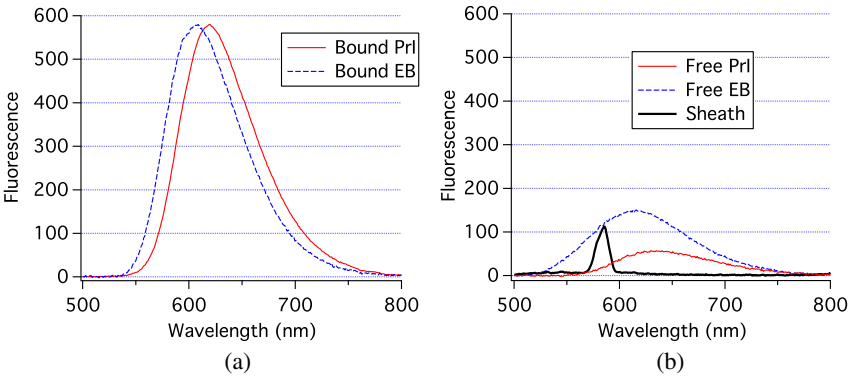

Fig. 2 (a) Spectra of ethidium bromide (dashed-blue) and propidium iodide (solid-red) bound to cells. These spectra are each averages of nearly 1000 cells and have been scaled to have the same maximum intensity in order to optimize visualization of spectral differences. (b) Spectra of free ethidium bromide (dashed-blue) and propidium iodide (solid-red). The spectrum of sheath, which is primarily the Raman spectrum of water is in black. Each spectrum is the average of hundreds of spectra.

collection was triggered on the initial falling voltage of a side-scatter event using the fast external trigger option of the camera. Background spectra, i.e., the spectra of the solutions the cells were in, were collected by setting the camera on internal trigger and then gating out all of the events that showed evidence of a cell being present. The Raman signal was collected with only sheath in the flow cell, using an internal trigger with no sample being injected. Spectral information was converted to ASCII for offline analysis.

2.4 *Data Analysis*

Data analysis was performed with Igor Pro 6.1. The forward-scatter and side-scatter time traces were fit to Gaussians from which peak height and width were extracted. The spectra were analyzed by two different methods and a noise-reduction technique was demonstrated, all of which are described below.

2.4.1 *Gating*

Gating can be performed using the scatter signals, as well as the spectra. Side scatter and forward scatter width and time were used to gate out outliers. Spectra of flow check beads are easily distinguished from those of the cells, due to the wavelength shift and different spectral shape, and were gated out on the rare occasions that they appeared in cell experiments due to sample carryover.

When the EMCCD is triggered, data readout begins after the set exposure time (60 μs). We have found that for up to 4 ms after the camera trigger, light incident on the camera can be collected and become part of the signal. Therefore, the time traces of forward-scatter and side-scatter are examined (with an automated procedure) for events within 4 ms of a trigger event. These "near doublet" events are gated out and accounted for the vast majority of the events that were gated out. A total of about 25% to 30% of the events were gated out.

2.4.2 *Fitting to basis/component spectra*

The methods of fitting multicomponent spectra to basis are best explained using cells as an example. When cells are multiply stained, the spectrum of each cell is a linear combination of the stains bound to the cells, any intrinsic signal from the cells, the solutions the cells are in, and the sheath. Measurement of the sheath reveals that our instrument measures the Raman spectrum of water and this is one of the basis spectra used. Free PrI and free EB fluorescence have a different emission spectrum than when they are bound to DNA in cells. Therefore, fluorescent spectra were obtained of each solution the cells were in.

Example basis (component) spectra are shown in Fig. 2. Averaged spectra of EB and PrI bound to cells are show in Fig. 2(a). Averaged spectra of solutions of free PrI and EB, as well as of the PBS sheath, are shown in Fig. 2(b). The Raman/Sheath contribution was subtracted out of the PrI and EB spectra and all spectra have had a constant subtracted.

Equation (1) shows the equation used to fit the individual cell spectra. The fit coefficients are c_0, c_1, c_2, c_3, and c_4. $E(\lambda)$ is the spectrum of EB bound to cells. $P(\lambda)$ is the spectrum of PrI bound to cells. $S(\lambda)$ is the spectrum of the solution the cells are in. $R(\lambda)$) is the spectrum of the sheath that is primarily a Raman band of water. χ^2 was optimized using the Levenberg-Marquardt algorithm and a non-negativity constraint was applied to all fit coefficients. Examples of cell spectra, the fit, and the contributions of each basis spectra to the fit are shown in Fig. 3. One cell shows a large EB contribution, while the other shows a large PrI contribution. The cells had been washed and there was very little dye in the solution surrounding the cells, consequently the solution background spectrum is very weak. A constant (determined using the data from 400 to 480 nm) was subtracted from the plotted cell spectra.

$$C(\lambda) = c_0 + c_1 E(\lambda) + c_2 P(\lambda) + c_3 S(\lambda) + c_4 R(\lambda). \quad (1)$$

2.4.3 *Spectral noise reduction*

Principle component analysis (PCA) was used to decompose a set of spectra. The spectra were then reconstructed using a small set of principle components that describe most of the variance in the data with a limited noise contribution.

2.4.4 *Spectral analysis without full knowledge of component spectra*

Alternating least squares (ALS) is a multivariate curve resolution (chemometric) technique for determining pure component information from multicomponent systems.[2] To obtain unambiguous results, constraints must be used. Non-negativity constraints were used for both the fluorescence spectra and the

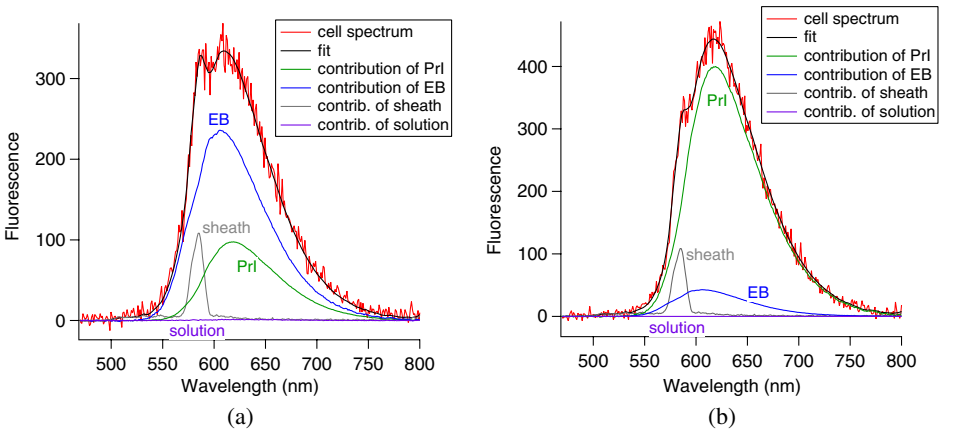

Fig. 3 Cell spectra, their fits and the contributions of the basis spectra to the fits. (a) A cell with more EB than PrI. (b) A cell with more PrI than EB.

concentration coefficients. Unimodality constraints were also used for the spectra. The spectra of the sheath was provided to the ALS algorithm and constrained not to change. The initial guesses for fluorescence spectra were Gaussians with peak and width information approximated from information about DNA-bound propidium iodide and ethidium bromide spectra that is readily available on the internet. All spectra were baseline-corrected so that average intensity from 397 to 470 nm was 0 before ALS analysis. ALS analysis was run until the average change in the EB fluorescence intensity (concentration coefficients) was less than 0.0003% and the average change in the PrI fluorescence intensity (concentration coefficients) was less than 0.0002%.

3 Results

Measurement of the linewidth of a 532 nm laser scattered from a flow check bead demonstrated that the spectral resolution is better than 1.5 nm and the spectral calibration had an absolute accuracy of ~1 nm.

3.1 *Polystyrene Beads*

Results from measurement of flow check beads are shown in Figs. 4–6. A side-scatter signal results in a negative voltage, therefore the three example side scatter traces shown in Fig. 4(a) are negative. The corresponding forward-scatter traces are shown in Fig. 4(b). There is some baseline variation for the forward-scatter signal. However, this variation does not affect the data quality, as each of the forward- and side-scatter traces was fit to a Gaussian plus a constant from which the peak height and width were extracted. Representative spectra from a sample of flow check and align flow beads are shown in Fig. 5(a). Two spectra of individual flow check beads are shown and two spectra of individual align flow beads are shown. Comparison of these spectra in red and black shows that there is strong spectral overlap. A spectrum of two flow checks beads simultaneously passing through the excitation laser is also shown. All spectra shown are processed only by subtraction of a constant.

To facilitate comparison of this instrument with a conventional instrument, the coefficient of variation (CV) of the fluorescence intensity from flow check beads from 564 to 606 nm was calculated and found to be 5% for the data set presented. For some data sets, the CV was smaller by more than a factor of 2. This calculation simulates the use of a common 585 ± 21 nm filter on a conventional flow cytometer.

When a mix of flow check and align flow beads were run, the beads were easily separable based on forward-scatter height and side-scatter height, as shown in Fig. 6(a). The beads were also easily separable based on their spectra. Each spectrum was fit to Eq. (2), where $F(\lambda)$ is the average spectrum of flow check beads run earlier, $A(\lambda)$ is the average spectrum of align flow beads run earlier, and $R(\lambda)$ is the average spectrum of the sheath. All three spectra are shown in Fig. 5(b). The coefficients c_0, c_1, c_2, and c_3 are determined from each fit. The fit coefficient for the flow check beads, c_1, is plotted versus the fit coefficient for the align flow beads, c_2, in red in Fig. 6(b). To evaluate the accuracy

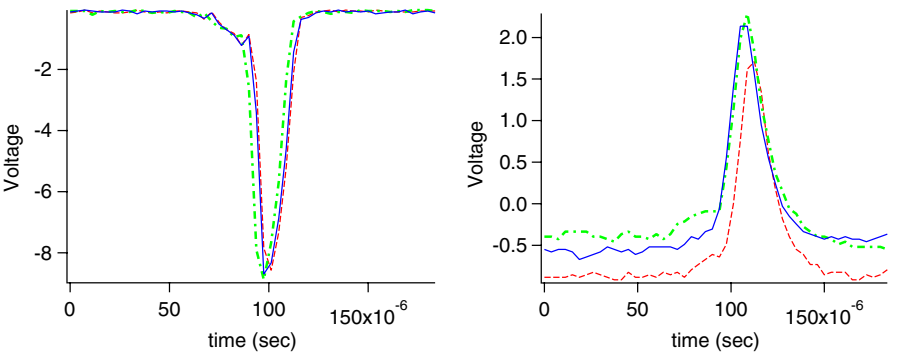

Fig. 4 Raw side scatter (a) and forward scatter (b) time traces from measurements of flow check fluorospheres. Traces from a single event have matching colors and line types.

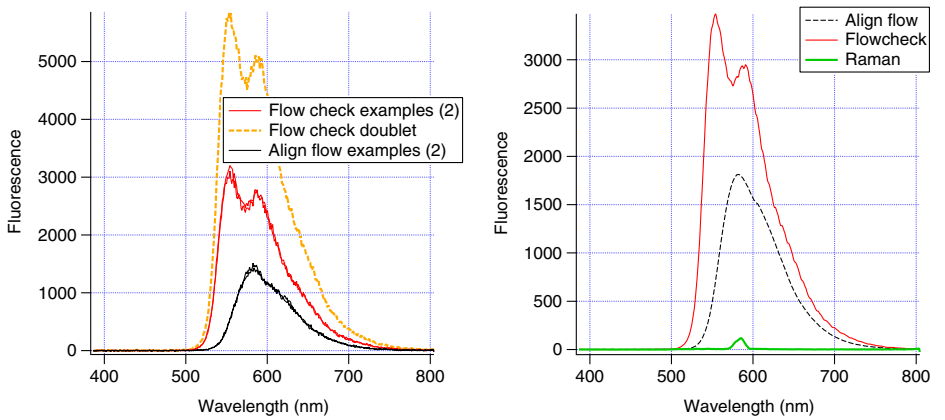

Fig. 5 (a) The two black spectra are align flow beads while the two red spectra are flow check beads. The yellow (top) one is a doublet of flow check beads. (b) Averaged spectra of flow check and align flow beads and Raman/Sheath.

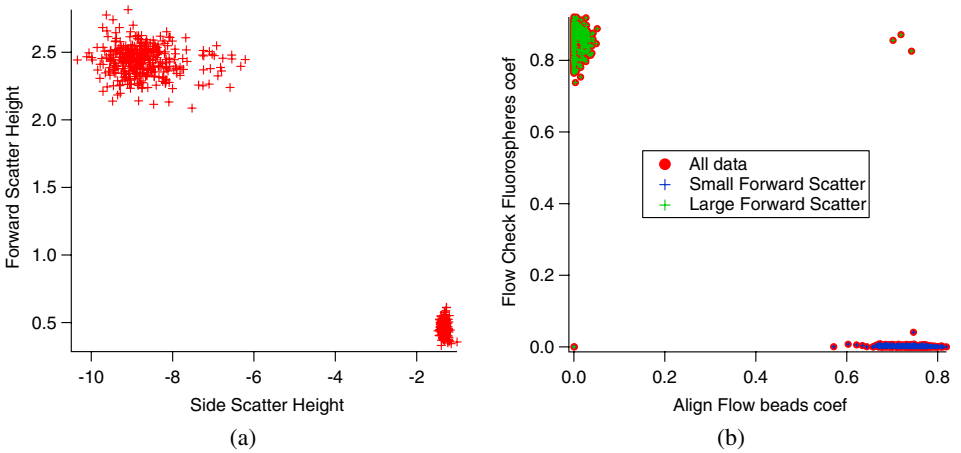

Fig. 6 (a) Forward scatter height versus side scatter height for a mix of flow check and align flow beads. Side scatter is a negative signal, so stronger side scatter is more negative. The flow check beads are the population in the upper left corner and the align flow beads are the population in the lower right corner. (b) Fit coefficient for the flow check beads versus the fit coefficient for the align flow beads.

of this separation, the data from cells with large forward scatter [i.e., the top left group in Fig. 6(a)] are overlaid in green and data from cells with small forward scatter overlaid in blue [i.e., the bottom right group in Fig. 6(a)]. Out of 643 data points, there are five beads that were not categorized the same way by scatter and spectral fluorescence analysis, two at the origin and three at the top right of the graph. Of the two points at the origin, one is the point on Fig. 6(a) with the smallest side scatter and could have been gated out. The three at the top right of the graph are likely doublets of a flow check and an align flow bead. All three points have high forward scatter and intense side scatter, in fact one is the point in Fig. 6(a) with the highest forward scatter. Because align flow beads are so much smaller than flow check beads, an align flow bead stuck to a flow check bead will not change the scatter significantly.

$$C(\lambda) = c_0 + c_1 F(\lambda) + c_2 A(\lambda) + c_3 R(\lambda). \qquad (2)$$

3.2 *Cells*

Results of a set of experiments using cells stained with PrI and EB are shown on a density plot in Fig. 7. The x-axis is the fit coefficient for the EB basis spectra multiplied by the area under the peak of the EB basis spectra (601.3 to 612.9 nm). The y-axis is the fit coefficient for the PrI basis spectra multiplied by the area under the peak of the PrI basis spectra (612.9 to 624.4 nm). The color shade represents the log of the number of cells. Cells stained only with EB are shown in shades of blue and have strong EB fluoresence. Cells only stained with PrI are shown in shades of green and have strong PrI fluorescence. Cells singly stained with EB and cells singly stained with PrI were mixed. Measurements taken ~3 min after mixing are shown in red. Measurements ~45 min after mixing are shown in cyan. At only 3 min after mixing, it is clear that both dyes are dissociating from and then rebinding to the cells. For example, the initially PrI stained cells have lost some PrI stain and gained some EB stain. At 45 min all cells have a similar proportion of EB and PrI bound.

3.3 *Noise Reduction with Principle Component Analysis*

The first four principle components of a PCA analysis of the measurements made 3 min after mixing, are shown in Fig. 8. The first three principle components clearly contain spectral information. The fourth principle component is noise, as are

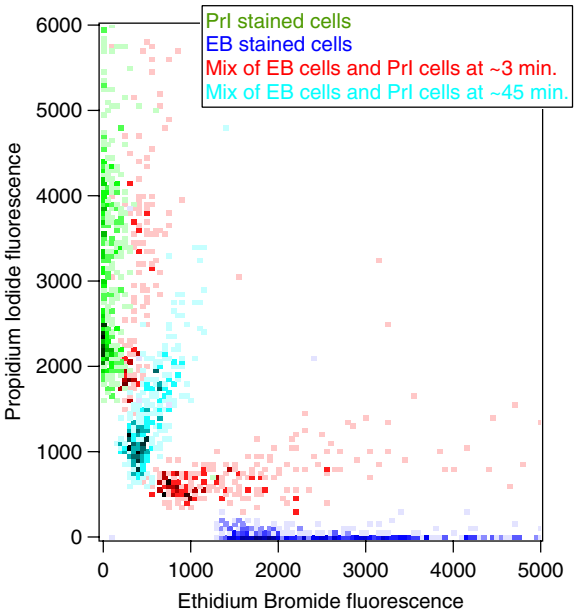

Fig. 7 Density plots from four samples with the density of cells represented by the darkness of the colors. Cells stained with only EB are blue. Cells stained with only PrI are green. These two cell populations were washed and mixed. Measurements made ~3 min after mixing are red. Measurements made ~45 min after mixing are light blue.

all of the higher principle components. The spectral data were remade using only the first three principle components. An example is shown in Fig. 9(a), which demonstrates the resultant noise reduction. To assess whether significant artifacts were introduced by the reconstruction, the reconstructed spectra were fit to basis spectra and the results compared to fits of the original spectra. The results in Fig. 9(b) show that the spectral fits do not change significantly.

3.4 *Potential for Automated Analysis Without Running Compensation Samples*

The starting and final spectra for the ALS analysis are shown in Fig. 10(a) where they can be compared with the basis spectra used earlier for fitting the data. The starting spectra are Gaussians and clearly have a different shape than the basis spectra. The final spectra are quite similar to the basis spectra. The PrI spectra is slightly red-shifted compared to the basis spectra. The shape of the EB spectra deviates slightly from the EB basis spectra, especially where it overlaps with the Raman spectra. The relative fluorescence intensities obtained from the ALS analysis are compared to earlier analyses in Fig. 10(b). The results are quite similar, however, the ALS results show decreased EB and increased PrI. The ALS analysis uses fewer basis (component) spectra to describe the measured spectra, because the spectrum of the solution the cells were in was not included in the ALS analysis. As Fig. 3 illustrates, the contribution of this spectrum was quite small. Nonetheless, to

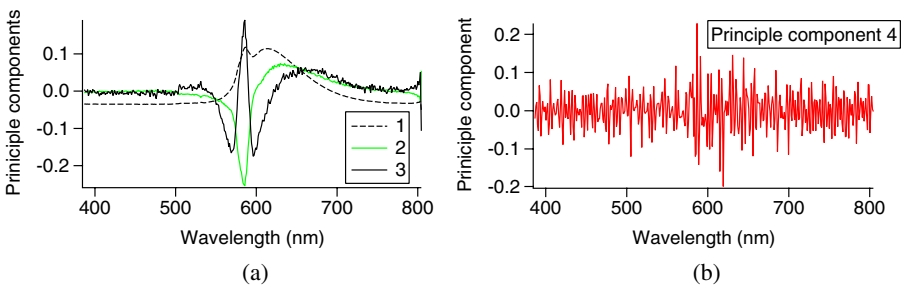

Fig. 8 Results of a PCA analysis of the spectra of the sample measured 3 min after mixing cells individually stained with PrI and EB. (a) The first three principle components (b) The fourth principle component.

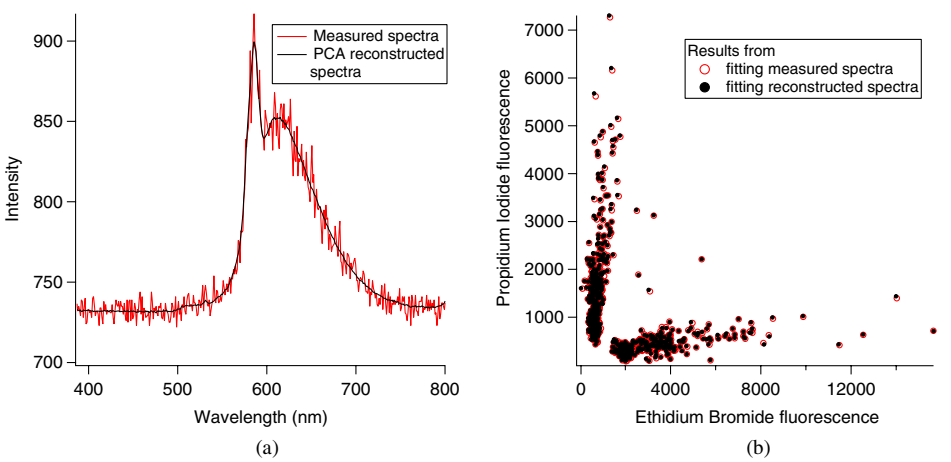

Fig. 9 (a) Comparison of a measured spectra with a PCA reconstructed spectra. (b) Results of fitting the measured data set compared with results of fitting the reconstructed data set.

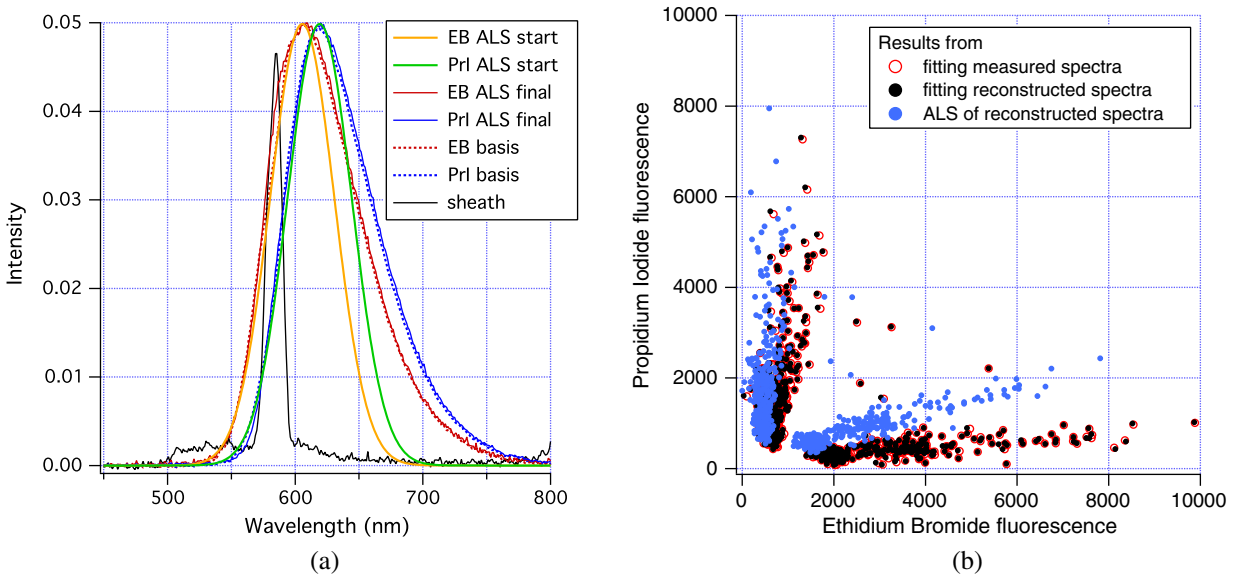

Fig. 10 (a) The Gaussian starting spectra for the ALS analysis are shown in orange and green. After 12,000 ALS iterations, the ALS spectra are in solid red and blue. The measured basis spectra are shown in dotted red and blue lines. The measured sheath spectrum is black. (b) Comparison of fluorescence contributions from EB and PrI to individual spectra obtained from fitting the data to component spectra and from ALS. The black dots and red circles are the same data shown in Fig. 9(b), however, the scales have been changed.

assure that not using the solution spectra was not the cause of the differences in Fig. 10(b), the spectra were fit without using the solution spectra. The lack of the solution spectra in the ALS analysis was not the cause of the differences in Fig. 10(b) (data not shown).

4 Discussion

The ability to separate a cell sample into two populations, both of which had fluorescence contributions from propidium iodide and ethidium bromide, demonstrates that this instrument and the analysis methods are able to quantify relative fluorescence of two spectrally similar dyes on individual particles. These two dyes are separated by only 12 nm and have full-width half-maxima of about 80 nm. There is clearly a potential to measure ~15 fluorophors accurately and simultaneously. With a grating optimized to the excitation, a 400-nm wide detection range would be available. Assuming emission spectra of a similar width to EB and PrI, there could be 15 spectral peaks spaced 20 nm apart over a 300-nm range (leaving 50 nm on the short and long wavelength ends). With narrower emissions available with quantum dots even more spectra could be measured.

The data-fitting methods used in this work effectively reduce high frequency noise if the basis spectra themselves are fairly noise-free. As seen in Fig. 3, the fits to the data look like noise-reduced spectra. The measurement of high resolution spectra also enables the use of principle component analysis to significantly reduce noise without any knowledge of the basis spectra. The reconstructed spectra were much cleaner than the original spectra, yet still contained their spectral information.

One of the challenges/drawbacks to multiparameter flow cytometry is compensation. In addition to measurement of the samples of interest, pure component samples must be measured. If 16 fluorophors are measured, then 16 pure component samples must be prepared and measured. (Other sample choices for compensation have been discussed in the literature and may have advantages, but all require the measurement of the same number of samples as there are components.)[3] Consequently, a method that does not need compensation would be highly advantageous. The ALS analysis presented here demonstrates that full spectrum flow cytometry could facilitate the implementation of multiparameter flow cytometry with few or no compensation samples. The data set used here is intrinsically a difficult one for ALS analysis due to the fact that the Raman spectrum of water overlaps very strongly with fluorescence from EB. Characterizing and optimizing ALS and other multivariate curve resolution methods for application to flow cytometry will be a significant undertaking that should be performed with improved instrumentation.

The data presented here demonstrate the potential of our experimental approach to the measurement of full spectra, however, there are improvements to be made in the instrumentation that are being facilitated by improvements in charge coupled device (CCD) and laser technology. The detector used was relatively old and data readout was quite slow. Data were collected at a rate of only about 68 events/s and since about 25% of these events were gated out due to the slowness of CCD readout, the real data rate was only about 50 events/s. Much faster readout rates are now available from multiple EMCCD manufacturers that have the potential to increase the event rate by more than an order of magnitude. The instrument used was not optimized for the detection of weak fluorophors. A simple increase in the intensity of excitation would allow measurement of weaker fluorophors. However, there would still be a problem with the dynamic range of the system. The EMCCD we used had a 12-bit A/D (4096 counts) and all spectra had a baseline of about 730 counts and the noise was at least 10 counts. Consequently, relative fluorescence changes of only about a factor of 100 to 200 could be measured by the instrument in its current configuration. In order to measure both weak and strong fluorophors in the same sample a newer 16-bit A/D EMCCD should be used. The current instrument used only one excitation

channel. Adding other excitation channels will require addition of new, smaller, lasers and some redesign of the optical train.

Other reports of full-spectrum flow cytometry measurements have been published including a 32-channel PMT-based system.[4] This instrument used a grating for wavelength dispersion, a 32-channel multianode linear PMT array for light detection and a custom high-speed data acquisition system. The data reported in the paper using five fluorophors were taken at a rate of ~1000 samples/s. A disadvantage of the initial implementation of the system was that correlation between wavelength and channel number was difficult. The paper stated that correspondence between the 32 channels and the collected wavelengths was "estimated." A 32-channel PMT-based instrument for spectral flow cytometry is currently being developed by Sony. With only 32 channels, this instrument will have less spectral resolution than a CCD-based system.

A few other spectral instruments have been recently reported in the literature designed for types of Raman spectroscopy.[5–8] These instruments use a similar design to the one described here that implements a spectrograph with attached high-sensitivity CCD camera. Most of these instruments have different design criteria than the rapid measurement of multiparameter spectra; they were designed to detect weak signals and consequently some use long transit times, e.g., 200 μs to 1 ms.[7] One of these instruments[5] is the predecessor of the prototype instrument described in this paper. An exception to the long transit times, is a Union Biometrica COPAS Plus instrument to measure spectra of large particles.[8] Excitation pulse widths were typically only 10 μs. As with our instrument, sample rates were limited by the CCD readout times. The technical note published on this instrument did not evaluate the ability of the instrument to resolve closely spaced fluorophors nor were coefficients of variation published.

Very recently the ability of a spectral flow cytometry instrument to quantify fluorescence from overlapping fluorophors was evaluated.[9] Individual quantum dot spectra were reportedly 'readily identified' in spectra from beads stained with six quantum dots. Spectral fits were not shown in the paper nor is correct identification quantified, but rather the reader is left to estimate it from the figures. Those quantum dot emission spectra were better separated than the emission spectra used in our work, quantum dot peaks are at 525, 565, 585, 605, 665, and 705 nm. Additionally, the spectral widths were about 40 nm narrower with the exception of the 705 nm quantum dot. When dyes with more spectral similarity were used correct identification was difficult for even singly stained particles when the sample contained particular dye combinations. The paper also reported (in the supporting information) CVs for quantum dots that were at least a factor of four greater than the CVs reported in the results section here for flow check beads.

5 Conclusions

A CCD-based flow cytometer for the measurement of full spectra was implemented and characterized. The spectral resolution was better than 1.5 nm and the CV for fluorescence from flow check beads was 5% or better. Full spectral measurement facilitates new analysis methods. Fitting to component spectra was performed for both bead samples and for cell samples. Separation of flow check and align flow beads, which have similar spectra, was nearly identical using the spectral or scatter analysis. The scatter analysis appears to have misclassified three instances of coincident flow check and align flow beads. In addition, no fluorescence was measured for two beads.

Mixes of cells stained with ethidium bromide or propidium iodide were measured at different timepoints after mixing. Spectral analysis by fitting to component spectra demonstrated that the contribution of these 12 nm separated emission spectra could be separately quantified and the kinetic process of the samples becoming homogeneous due to fluorophor dissociation and rebinding could be observed. Principle component analysis was used to reduce noise and alternating least squares was used to analyze one set of noise-reduced data. With the use of prior information to estimate spectral position and width and with appropriate constraints, the ALS analysis yielded spectra similar to the measured component spectra and fluorescence contributions to individual spectra similar to that obtained by spectral fitting.

Spectral flow cytometers could facilitate significant improvements in multiparametric flow cytometry. With spectral detection there is never any need to change the collection filter. Background (e.g., solution spectra) are readily observed and can be identified. With current advances in CCD technology, readout rates of CCD-based systems will facilitate analysis rates of about 1000 particles per second. With the implementation of multivariate curve resolution techniques made possible by full spectrum flow cytometry, the number of samples that need to be measured to account for spectral overlap could potentially be greatly reduced.

Acknowledgments

We thank Oana C. Marina for cell culture and James P. Freyer for useful discussions. Funding for this work was primarily provided by the Los Alamos National Flow Cytometry Resource funded by the National Center for Research Resources of NIH (Grant P41-RR01315) with some additional funding from National Institutes of Health (Grant CA071898). Versions of this paper without the PCA and ALS analysis were rejected by Cytometry A and subsequently by Optics Express in 2012. Some of the comments from those reviewers led to improvements in this paper.

References

1. M. Roederer et al., "8 color, 10-parameter flow cytometry to elucidate leukocyte heterogeneity," *Cytometry* **29**(4), 328–339 (1997).
2. A. de Juan and R. Tauler, "Chemometrics applied to unravel multicomponent processes and mixtures revisiting latest trends in multivariate resolution," *Anal. Chim. Acta* **500**(1–2), 195–210 (2003).
3. M. Roederer, "Compensation in flow cytometry," *Curr. Protocols Cytometry* **22**, 1.14.1–1.14.20 (2002).
4. G. Gregori et al., "Hyperspectral cytometry at the single-cell level using a 32 channel photodetector," *Cytometry Part A* **81A**(1), 35–44 (2012).
5. G. Goddard et al., "High-resolution spectral analysis of individual sers-active nanoparticles in flow," *JACS* **132**(17), 6081–6090 (2010).
6. C.H. Camp et al., "Label-free flow cytometry using multiplex coherent anti-Stokes Raman scattering (MCARS) for the analysis of biological specimens," *Opt. Lett.* **36**(12), 2309–2311 (2011).
7. D.A. Watson et al., "A flow cytometer for the measurement of raman spectra," *Cytometry Part A* **73A**(2), 119–128 (2008).
8. D.A. Watson et al., "Spectral measurements of large particles by flow cytometry," *Cytometry Part A* **75A**(5), 460–464 (2009).
9. J.P. Nolan et al., "Visible and near infrared fluorescence spectral flow cytometry," *Cytometry Part A* **83A**(3), 253–264 (2013).